

ANALYSIS ON COMPLEX HYPERSONIC FLOW DURING THE REENTRY OF EXPIRED SPACECRAFT

Zheng Han^{1,2}, Zhi-Hui Li^{2,3}, Shi-Yong Chu¹, Wen-Yuan Cheng¹, Chuan-Sheng Wang¹

¹Aviation Industry Development Research Center of China, Beijing 100029, China ²National Laboratory for Computational Fluid Dynamics, Beihang University, Beijing 100191, China ³China Aerodynamics Research and Development Center, P.O. Box 211, Mianyang 621000, China

Abstract

This research focus on an analysis of the complex hypersonic flow dynamics during the reentry of expired spacecraft, such as China's Tiangong-1, into the Earth's atmosphere. The study is motivated by the need to understand and predict the behavior of space debris to mitigate potential risks to both terrestrial and space-based assets. The investigation focuses on the flow patterns around the Tiangong-1 spacecraft's compartment at various angles of attack, elucidating the effects of the spacecraft's geometry on shock wave formation and flow disturbances. The study extends to the multi-body flow around debris fragments, particularly examining the influence of different shapes and configurations on aerodynamic interference and forces. The results demonstrate that the thermal-chemical non-equilibrium model significantly improves the accuracy of aerodynamic force predictions compared to the perfect gas model. Furthermore, the research reveals that debris interaction is substantial at close distances but diminishes at greater separations, suggesting a threshold beyond which debris can be modeled as independent entities for trajectory predictions. This study contributes to the field by providing a robust computational framework for simulating hypersonic flows around disintegrating spacecraft and offers insights into debris behavior that can inform space debris management and risk mitigation strategies. The findings are particularly relevant for the aerospace community, policymakers, and entities involved in space traffic management and environmental safety.

Keywords: The reentry of expired spacecraft, complex hypersonic flow, Navier-Stokes equation, Flow around multi-bodies.

1. Background

With the rapid development of aerospace technology, the number of long-serving spacecraft is increasing. When a large spacecraft in low Earth orbit reaches the end of its operational life, it gradually decays in orbit due to gravitational and atmospheric drag. As its altitude decreases, it eventually enters the atmosphere at an altitude of 120 km and undergoes a sequence of flow regimes including free molecular flow, rarefied transitional flow, slip flow, and continuum flow. This process involves reentry into a high aerodynamic environment at the first cosmic velocity, leading to structural thermodynamic responses, deformation, melting, ablation, and a continuous decrease in accumulated thermal energy [1-8].

After the service life, the spacecraft will experience thermal decomposition and ablation due to aerodynamic heating effects upon reentry into the atmosphere at hypersonic speeds. This results in multiple disintegrations of the spacecraft and the generation of debris fragments. Simulating the aerodynamic, thermal, and disturbance effects caused by the spacecraft and its debris fragments during reentry, as well as revealing the flow mechanisms involved, is crucial for predicting the dispersion range of the debris fragments, conducting numerical forecasts of the coverage area of reentry disintegration, reducing collision risks with other aerospace vehicles, and assessing the potential harm to human, financial, and ecological systems on the ground [9-14].

Therefore, our study addresses the critical bottleneck in accurately simulating hypersonic flow created by the multiple disintegrations of expired spacecraft re-entering near space, which

significantly impacts the prediction of the falling area of disintegration debris. In this study, we developed a solver for the thermochemical non-equilibrium Navier-Stokes (N-S) equations that considers the excitation of vibrational energy. Using the Tiangong-1 spacecraft as an example, we conducted flow simulation calculations for the Tiangong-1 compartment at different angles of attack. We compared the computational accuracy with and without considering the slip boundary flow theory correction. Additionally, we conducted numerical simulations for the multi-body flow around the debris of the Tiangong-1 spacecraft. The research on the simulation of multi-body flow mechanisms around different combinations was carried out with varied shapes and spacing.

2. Method

All computational simulations are conducted using an in-house CFD code developed by the authors. Additionally, this code incorporates MPI (Message-Passing-Interface) parallel technology to enhance efficiency and employs a local time marching method to accelerate the convergence of computations to a stable state.

The energy decay and deceleration of a spacecraft during its reentry and disintegration process after the end of its service life result in the conversion of its enormous kinetic energy into heat energy. This leads to the surrounding air entering a non-equilibrium flow state, with the occurrence of chemical reactions such as dissociation and displacement after the hypersonic flow shock wave. The characteristic time of these reactions can be compared to the flow characteristic time, and the energy modes of gas molecules, including translational, rotational, and vibrational modes, are excited. At this point, the complete gas Navier-Stokes equations are no longer sufficient to accurately simulate the flight state, and it is necessary to introduce a thermal-chemical non-equilibrium physical model into the governing equations [15-20].

Based on the three fundamental principles - mass conservation, momentum conservation, and energy conservation - the Navier-Stokes (N-S) Equations describing the multi-body flow around irregular debris in a near-space flight environment can be derived. The N-S equations for a multicomponent, two-temperature model and thermochemical reaction non-equilibrium flow in a three-dimensional rectangular coordinate system can be formulated as follows:

$$\frac{\partial Q}{\partial t} + \frac{\partial E}{\partial x} + \frac{\partial F}{\partial y} + \frac{\partial G}{\partial z} = \frac{\partial E^{v}}{\partial x} + \frac{\partial F^{v}}{\partial y} + \frac{\partial G^{v}}{\partial z} + \mathbf{S}$$
 (1)

where all variables are dimensionless, with respect to the characteristic length, incoming flow density and velocity of the object, respectively. \vec{Q} denotes conserved variables. \vec{F} , \vec{G} and \vec{H} are the inviscid vector flux in the three coordinate directions of x, y and z, \vec{F}_v , \vec{G}_v and \vec{H}_v are the viscous vector flux in three coordinate directions^[21-35].

In near space, the Knudsen layer on the aircraft surface has a thickness equivalent to the average free path of gas molecules. As a result, the N-S equations become inapplicable due to the significant discontinuous particle effects of rarefied gas, and the gas molecule velocity distribution function deviates considerably from the Maxwell equilibrium state because of the large flow field gradient near the wall. To solve the N-S equations outside the Knudsen layer on the aircraft wall, a reasonable mathematical model for slip boundary conditions in high-temperature multicomponent mixed gas surfaces can be constructed to correct the N-S equation solver for surface velocity slip and temperature jump. Based on the model developed by Gupta and using plate flow as an example, the model for air with a five-component slip boundary is provided as follows.

3. Model and Grid

The first computational models used in this study were based on the compartment of the Tiangong-1 target spacecraft, as shown in Figure 1. The wind tunnel tests were conducted using two scaled-down models with a reduction ratio of 2%. The total length of the models was $0.20289 \ m$, and the reference area of the models was $3.52566 \times 10^{-3} \ m^2$.

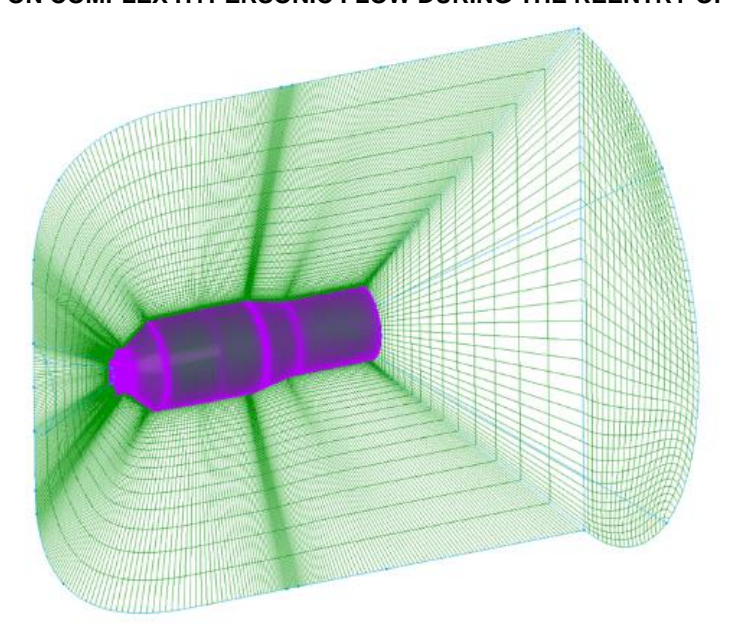


Figure 1 – The grids of the compartment of the Tiangong-1.

The second set of models in this paper are the multiple disintegrates of China's Tiangong-1 target aircraft uncontrolled fall reentry - propulsion gas cylinders. The propulsion gas cylinders are rotating bodies, which are composed of hemispheres and cylinders at both ends. The diameter of hemispheres at both ends is $D = 450 \ mm$ and the length of cylinder section is $L = 577 \ mm$.

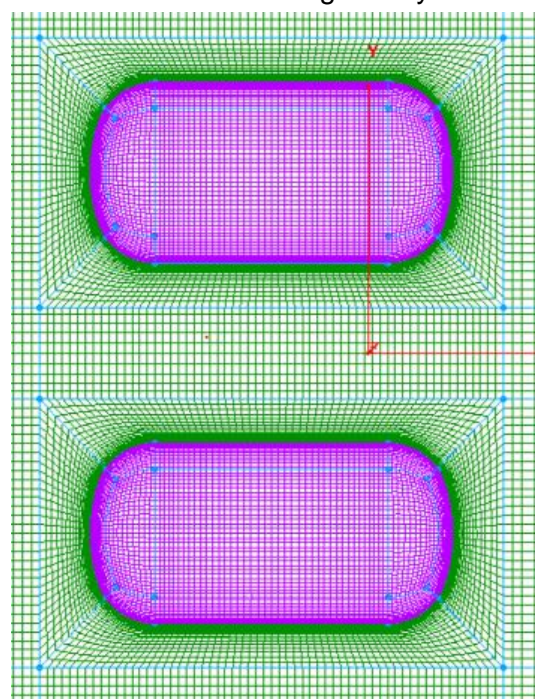


Figure 2 – The grids of propulsion gas cylinder.

4. Current Results

4.1 Results of simulation on hypersonic flow around the compartment of Tiangong-1 spacecraft

In this section, numerical simulations are conducted on the compartment formed after the uncontrolled reentry and disintegration of the Tiangong-1 target spacecraft. Different flow field patterns of dimensionless pressure and Mach number are plotted for different angles of attack (AoA) at 0°, 25°, 60°, 90°, and 120°, at a height of 65.2 km and Ma=12.5, as shown in Figures 3 and 4. The

figures provide a visual representation of the hypersonic flow field in the near-space flight environment. At an AoA of 0°, the irregular shape of the spacecraft causes disturbances, resulting in attached oblique shock waves and flow patterns. For flight AoA between 25° and 90°, the flow field exhibits certain detached shock waves. At AoA of 90° and 120°, the flow field displays the characteristics of attached oblique shock waves on the front and rear faces due to the irregular shape of the rear body.

Table 1 – Parameters of flow state around tiangong-1 target spacecraft's two cabins used low-density wind tunnel experiment and numerical simulation.

Sample	Altitude <i>H</i> (<i>km</i>)	Mach number M_{∞}	Total temperature T_o	Total pressure P _o (<i>MPa</i>)	Knudsen number $k_{n^{\infty}l}~(imes 10^5)$	Reynolds number $R_{e^{\infty}L}$ (\times 10 ⁵)
1	65.2	12.5	592	1.52	5.10	3.70
2	62.1	12.79	586	2.43	3.37	5.63

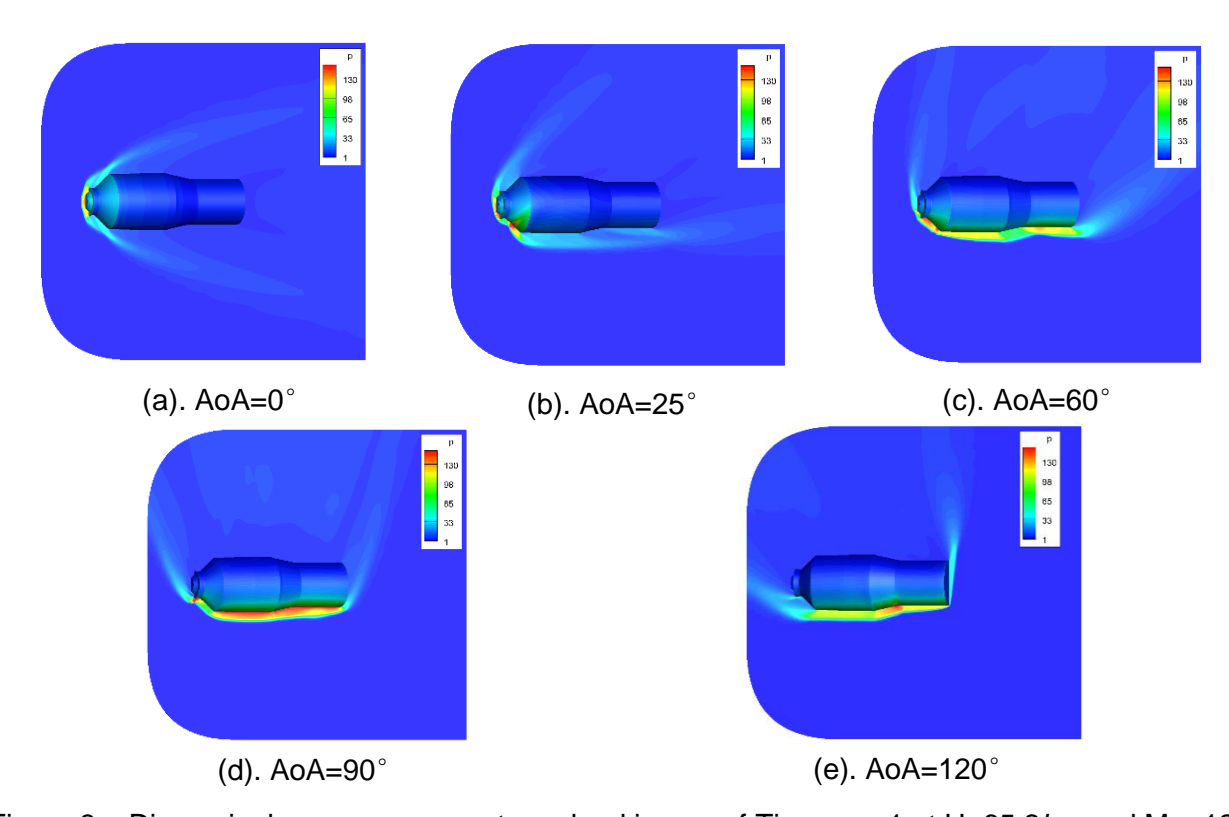
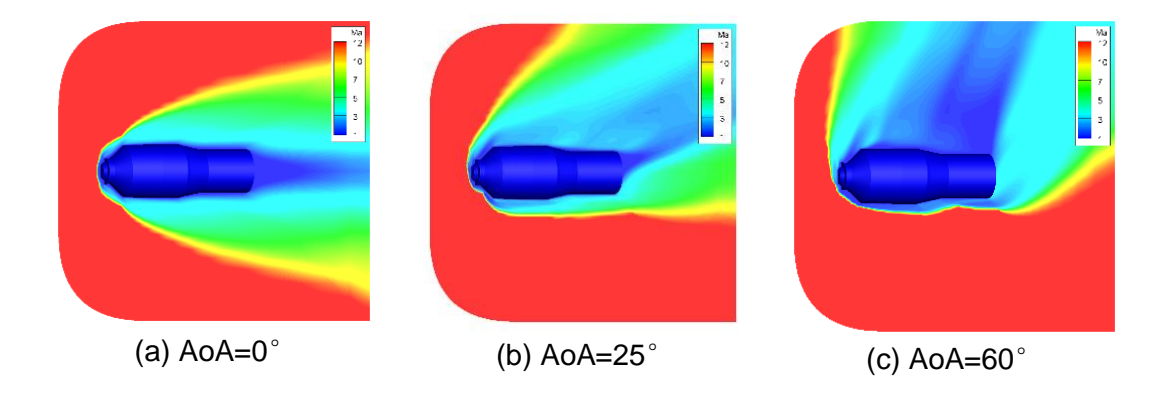


Figure 3 – Dimensionless pressure contour cloud image of Tiangong-1 at H=65.2km and Ma=12.5.



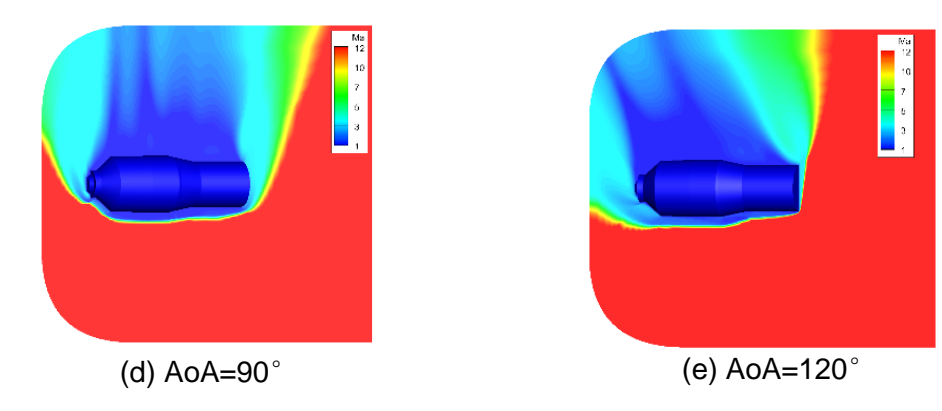


Figure 4 – Mach number contour cloud image of Tiangong-1 at H=65.2km and Ma=12.5.

In order to compare and analyze the characteristics of the flow field around irregular disintegrated objects in near space solved by numerical method based on N-S equations for perfect gas and thermochemical reaction with internal energy excitation, the pressure and Mach number contour of the flow field around the compartment at H=65.2km, Ma=12.5 and AoA=25° are shown in Figure 5 and 6, respectively. It shows that the flow structures in the two flow medium are similar with each other, and one detached shock wave is formed in perfect gas flow around two bodies, and is more away from the surface than that in the chemical reaction flow excited by internal energy. The reason is that the energy dissipation can induce chemical reaction, so that hypersonic detached shock wave layer thickens the surface flow on attachment, and it shows that the method presented is available and feasible.

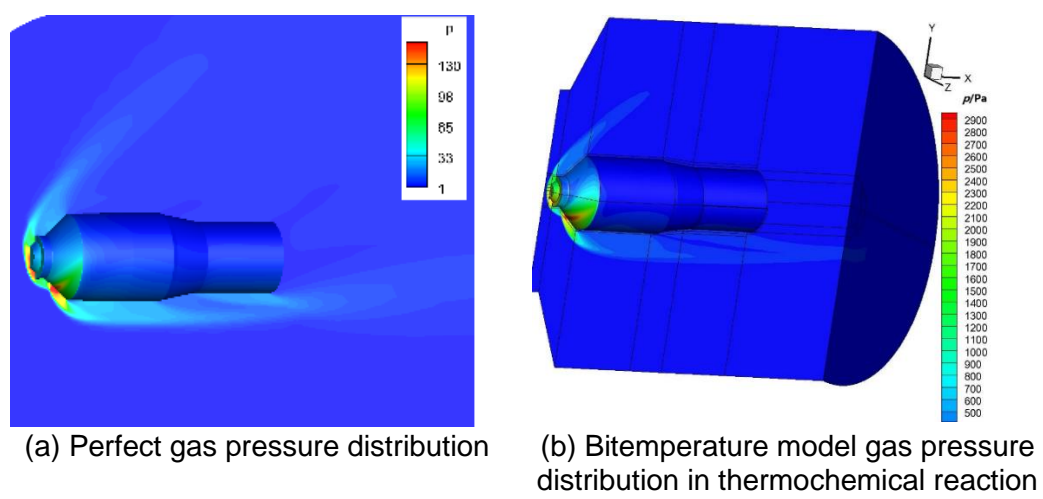


Figure 5 – Pressure contour cloud image of Tiangong-1 at H=65.2km, Ma=12.5 and AoA=25°.

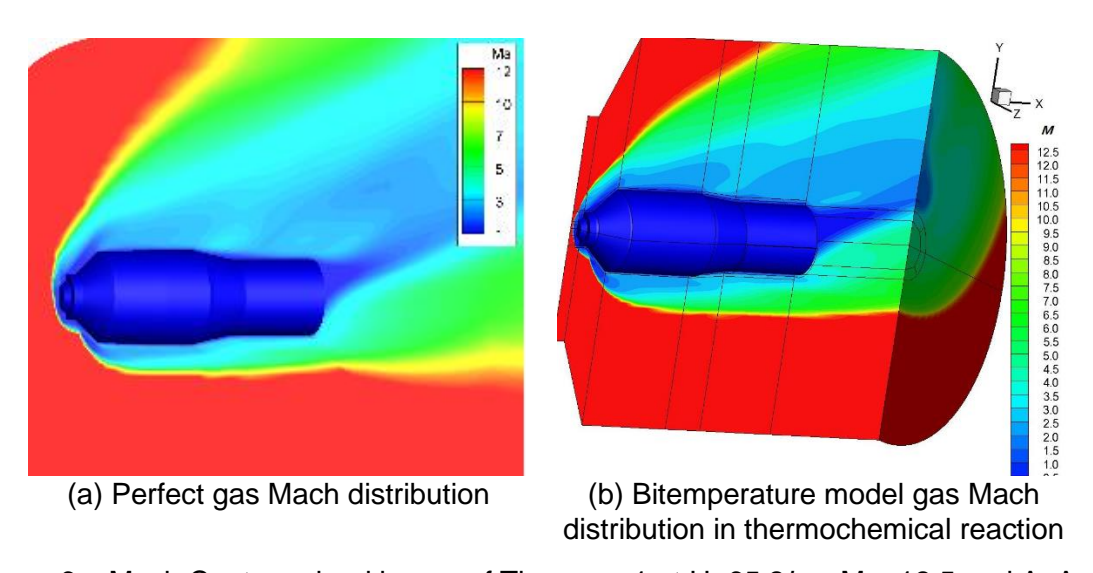


Figure 6 – Mach Contour cloud image of Tiangong-1 at H=65.2km, Ma=12.5 and AoA=25°.

Table 2 – Low density wind tunnel experimental state 2: H = 62.1km, $Ma_{\infty} = 12.79$, $Kn_{\infty} = 3.7 \times 10^{-5}$ calculation and test comparison

α	$C_{\scriptscriptstyle A}$	C_{N}	C_{m}	X_{cp}	$C_{\scriptscriptstyle L}$	$C_{\scriptscriptstyle D}$	C_L/C_D	Note
	0.8944	0.0000	0.0005	0.3255	0.0000	0.8944	0.0000	Wind tunnel tests
	0.88891	0.0000	0.0000	0.3006	0.0000	0.88891	0.0000	No-slip calculation
0	-0.61	-0.01	0.01	-7.65	-0.01	-0.61	-0.01	Calculation deviation (%)
	0.87303	0.0000	0.0000	0.3037	0.0000	0.87303	0.0000	Calculation of slip boundary flow
	-2.36	-0.01	0.01	-6.70	-0.01	-2.36	-0.01	Calculation deviation (%)
	0.9479	0.3276	-0.1111	0.3392	0.1580	0.9904	0.1595	Wind tunnel tests
	0.94337	0.33639	-0.10974	0.3244	0.16751	0.98705	0.1697	No-slip calculation
10	-0.48	2.68	1.22	-4.36	6.02	-0.34	6.39	Calculation deviation (%)
	0.92579	0.33293	-0.10801	0.3198	0.16718	0.96946	0.1724	Calculation of slip boundary flow
	-2.33	1.63	2.78	-5.72	5.81	-2.11	8.09	Calculation deviation (%)
	0.9883	0.6662	-0.2422	0.3635	0.2880	1.1566	0.2490	Wind tunnel tests
	0.98138	0.66484	-0.23427	0.3524	0.28885	1.14929	0.2513	No-slip calculation
20	-0.70	-0.14	3.27	-3.05	0.30	-0.63	0.09	Calculation deviation (%)
	0.96379	0.65803	-0.23158	0.3519	0.28874	1.13114	0.2553	Calculation of slip boundary flow
	-2.48	-1.23	4.39	-3.19	0.26	-2.20	1.53	Calculation deviation (%)
25	0.9632	0.8795	-0.3474	0.3950	0.3900	1.2447	0.3133	Wind tunnel tests
	0.94280	0.85658	-0.32992	0.3852	0.37803	1.21679	0.3107	No-slip calculation
	-2.12	-2.60	-5.03	-2.48	-3.07	-2.24	-0.08	Calculation deviation (%)
	0.93089	0.84977	-0.32684	0.3846	0.37644	1.20261	0.3130	Calculation of slip boundary flow
	-3.35	-3.38	-5.92	-2.68	-3.47	-3.38	-0.01	Calculation deviation (%)

Table 2 lists the flight altitude H=65.2km and 62.1km, the two states in the low-density wind tunnel experiment, implying the near-continuous slip flow zone. Due to the large scale of the two cabins of Tiangong-1 target aircraft, the corresponding Knudsen number $Kn_{\infty} = 5.1 \times 10^{-5}$, $Kn_{\infty} = 3.7 \times 10^{-5}$ are small and hence the flow is continuous. In order to analyze and compare the deviation between numerical results and experiment on aerodynamic moment coefficients in the above two experimental states, as numerical methods considering boundary slip effect of non-equilibrium flow surface at high temperature and that without considering surface slip, Table 2 gives the deviation compared with the experimental states 2 with H=62.1km, $Ma_{\infty}=12.79$, $Kn_{\infty}=3.7\times10^{-5}$, at angle of attack in the flight $\alpha = 0^{\circ}$, 10° , 20° , 25° . Using wall slip model and no slip conditions in this paper respectively, the numerical algorithms to solve the Tiangong-1 module two experiments state income aerodynamic moment coefficient calculation with the experimental deviation. It can be seen that maximum deviation is less than 7.65%, the rules to the large scale complex flow around two hull structure, even though Knudsen number $Kn_{\infty} = 3.7 \times 10^{-5}$ belongs to continuous medium flow at a minimum. Due to the flight altitude has reached the near-continuous transition zone, the maximum deviation between the aerodynamic force, torque and pressure center coefficient calculated by using N-S equation solver with high temperature non-equilibrium surface slip boundary effect and the lowdensity wind tunnel experimental data is 6.7%, which is less than the value calculated by N-S equation without slip. It shows that the development of N-S equation solver considering the modification of slip boundary conditions is more accurate and reasonable to calculate the aerodynamic force/moment of large scale irregular disintegrations in near space.

4.2 Results of simulation on flow around irregular multi-debris in near space.

In this section, the numerical simulation on the flow around two paralleled propelling bottles is carried out using the numerical algorithm that based on N-S equation and focuses on the problems of flow around irregular multi-body in near space. The Mach number contours are shown in Figure 7 when the mainstream Mach number is 3, the flying altitude is $40 \, km$ and the distance between the axes of two propelling bottles $\Delta y = 1.5D_{\odot} 2D_{\odot} 3.5D$. As is displayed in the figure, the detached shock waves are generated near the leading edge of each propelling bottle, which intersect with each other in the

flow region between two bottles, resulting in complex interference between Mach disk and the flow such as the intersection, reflection, and fusion of shock waves.

The distance between two propelling bottles has significant impact on the characteristics of the flow field. When $\triangle y=1.5D$, the detached shock waves generated near the leading edge of the bottles intersect with each other at X=-26mm (the stagnation point of the bottle is located at X=0mm), generating a clear Mach Disk. After intersection, transmitted shock waves impinge on the walls of the propellant cylinder, inducing shock wave-boundary layer interaction, leading to a sudden increase in the pressure near the debris wall, thus modifying the aerodynamic coefficients of the debris. When ∆y=2D, the detached shock waves are generated near the leading edge of each bottle and intersected with each other at X=143mm, the interference is still remarkable, generating obvious reflected shock waves that are similar as those in the hypersonic inlet. As $\triangle y$ continue to increase, when it reaches 3.5D, the intersection of two shock waves moves further downstream. They intersect at X=640mm and the transmitted shock waves directly propagate to the downstream so that the interference of the shock waves on the debris is wakened. As is displayed in Table 3, the minimum distance between the shock waves and the stagnation point of the bottle remains at 109mm, indicating that the position of the axes of the detached shock waves in the front of the paralleled propelling bottles will not change with the variation of the distance between two bottles, in this regard, the interference of the flow field has no influence on the detached shock waves. When $\triangle y$ is sufficiently small, almost equal to D, the two propelling bottles are combined into a single object. In this way, the flow becomes similar to that of a single body. Conversely, when $\triangle y$ is sufficiently large, the flow structures of two propelling bottles will not affect each other, as a result, the two shock waves develop independently.

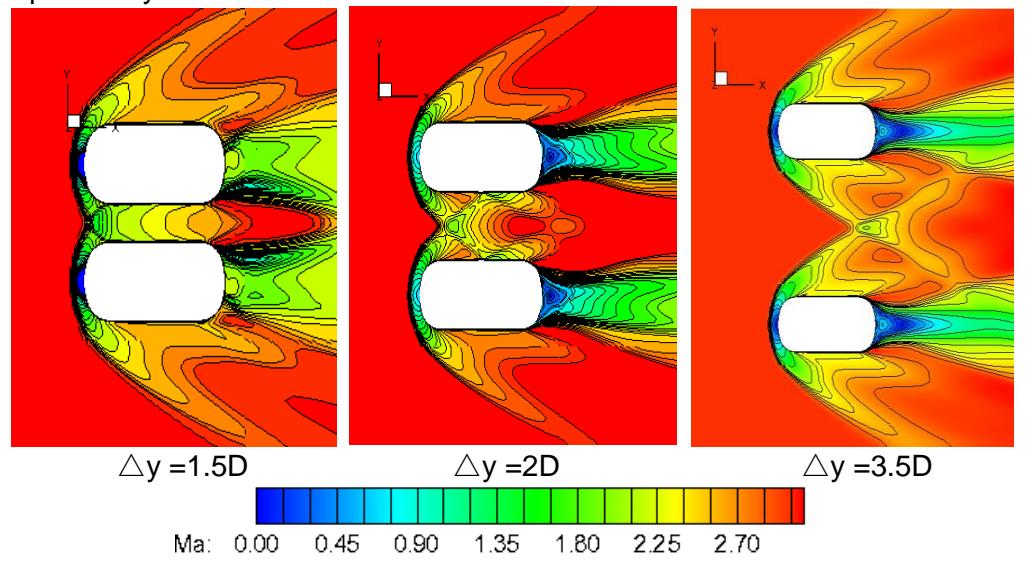


Figure 7 – Mach number contours when propelling bottles are placed paralleled with different $\triangle y$.

In order to quantitatively analyze the flow around paralleled propelling bottles placed with different spacing, the axial and normal force coefficient on one of the bottles when $\triangle y=1.5D$, 2D and 3.5D is listed in Table 3. As is shown in the table, with the increase of $\triangle y$, the magnitude of axial force coefficient remains almost the same, because it mainly influenced by the detached shock waves near the leading edge of the bottle. When y=3.5D, the axial force coefficient decreases remarkably, this is because that when the position of the intersection of shock waves moves downstream, the transmitted shock wave directly enters the downstream and no longer affects the flow field near the wall of the propelling bottles. When $\triangle y=1.5D$ or 2D, the shock wave interact strongly between two propelling bottles, resulting in a significant multi-body interference, thus improving the normal force coefficient. Since the normal force coefficient is mainly due to the interference of the paralleled propelling bottles, which is not obvious when $\triangle y=3.5D$, the order of magnitude of the normal force coefficient in that condition is only 10^{-4} . Moreover, the shock wave interaction results in a significant change in the characteristics of the flow field. When $\triangle y$ is small, the mutual interference of two debris is strong, and the changes of the flow around the debris can't be explained simply by analyzing the

flow around a single debris. When $\triangle y=3.5D$, the force coefficients of a single propelling bottle, especially the normal force coefficient, are significantly reduced. The detached shock waves intersect with each other and generate two transmitted shock waves that directly propagate downstream. In this condition, the interference between two debris is substantially weakened so that its effect on the flow field can be neglected, thereby the forecast of the path line of the debris can be conducted through the independent numerical simulation on each debris.

Table 3 – Minimum distance between shock wave and stagnation point of debris and location of intersection of shock waves.

interesection of effect traveer					
△y	1.5D	2D	3.5D		
Minimum distance	109mm	109mm	109mm		
Position of intersection	X=-26mm	X=143 <i>mm</i>	X=640mm		

Table 4 – Axial and normal force coefficient of paralleled placed propelling bottles when Ma=3 and the altitude is 40km.

the aithtude is 40km.					
∆у	1.5D	2D	3.5D		
Axial force coefficient	8.80E-02	8.73E-02	7.55E-02		
Normal force coefficient	3.67E-02	3.22E-02	1.06E-04		

5. Current Conclusion

This study focuses on the disintegration process of an expired spacecraft during reentry into the atmosphere. A numerical simulation is conducted using the Navier-Stokes method that considers thermochemical non-equilibrium to analyze the disintegrated debris of the Tiangong-1 spacecraft. This study mainly concludes two important findings. First, the numerical algorithm for solving the N-S equations for thermal chemical reactions with internal energy excitation has more advantages and computational accuracy than the N-S equations for perfect gases when solving the flow field around irregular dissociative objects in near space, especially in improving the accuracy of aerodynamic force calculations by at least 15% or more. Second, the results show that irregular debris, e.g. propelling cylinder, show strong interaction when their distance is $\triangle y < 3D$ or $\triangle x < D$, and significant changes can be found in flow and aerodynamic characteristics. However, the interaction is negligible if the distance increases to a certain magnitude. When the distance between the debris in the near space reaches a certain level, the influence of mutual interference can be ignored, and debris can be regarded as two separate pieces of disintegrated wreckage to be carried out the engineering application design of numerical prediction software for aerodynamic fusion ballistic flight track landing area.

6. Contact Author Email Address

mailto: han10098@126.com

7. Copyright Statement

The authors confirm that they, and their company or organization, hold copyright on all of the original material included in this paper. The authors also confirm that they have obtained permission, from the copyright holder of any third party material included in this paper, to publish it as part of their paper. The authors confirm that they give permission, or have obtained permission from the copyright holder of this paper, for the publication and distribution of this paper as part of the ICAS proceedings or as individual off-prints from the proceedings.

References

- [1] Fritsche L., Geppert U., Riede W. End-of-life disposal of high area-to-mass ratio (HAMR) objects and the related fragmentation environment. Acta Astronautica, Vol. 65, No. 1-2, pp. 247-262, 2009.
- [2] Bronson M. R., Hager J. D., Wercinski P. F., Poteet C. C. A probabilistic-based approach to spacecraft reentry survivability assessment. Acta Astronautica, Vol. 76, pp. 58-64, 2012.
- [3] Corliss J. M., Palmer G., Rudolph T. Analysis of spacecraft breakup in the atmosphere: The Shuttle–Columbia accident. Acta Astronautica, Vol. 152, pp. 516-524, 2018.

- [4] Chen Y. K., Chen P. H. Aerothermodynamics of spacecraft and composites during atmospheric reentry: A review. Journal of Materials Science, Vol. 48, No. 6, pp. 2273-2295, 2013.
- [5] Neely A. J., McIntyre T. J., Milthorpe J. F., Zander F. Heating of ablative materials under shock layer radiation. International Journal of Thermal Sciences, Vol. 137, pp. 224-238, 2019.
- [6] Lips T., Braun R. D. Uncertainty quantification of ablative material response. Journal of Spacecraft and Rockets, Vol. 55, No. 2, pp. 313-328, 2018.
- [7] Johnson N. L., Krisko P. H. The increasing orbital debris collision hazard: Steady state? Advances in Space Research, Vol. 45, No. 9, pp. 1077-1084, 2010.
- [8] Poovathingal S., Stern E. C., Nompelis I., Schwartzentruber T. E., Candler G. V. Nonequilibrium flow through porous thermal protection materials, Part II: Oxidation and pyrolysis. Journal of Computational Physics, Vol. 380, pp. 427-441, 2019.
- [9] Han Zheng, Li Zhihui, Bai Zhiyong, Li Xuguo, Zhang Jiazhong. Study on Numerical Algorithm of the N-S Equation for Multi-Body Flow around Irregular Disintegration in Near Space. Aerospace, Vol. 9, No. 7, pp. 347, 2022.
- [10] Han Zheng, Li Haiyan, Li Zhihui, Luo Wanqing, Li Ming, Zhang Jiazhong. Numerical Simulation of Chemical Non-equilibrium Flow for Ablative Flow Fields in Near Space. Journal of Environmental Accounting and Management, Vol. 11, No. 3, pp. 271-283, 2023.
- [11] Liang Jie, Li Zhi-Hui, Li Xu-Guo, Shi Wei-Bo. Monte Carlo Simulation of Spacecraft Reentry Aerothermodynamics and Analysis for Ablating Disintegration. Communications in Computational Physics, Vol. 23, No. 4, pp. 1037-1051, 2018.
- [12] Li Zhi-Hui, Ao-Ping Peng, Qiang Ma, Lei-Ning Dang, Xiao-Wei Tang, Xue-Zhou Sun. Gas-Kinetic Unified Algorithm for Computable Modeling of Boltzmann Equation and Application to Aerothermodynamics for Falling Disintegration of Uncontrolled Tiangong-No.1 Spacecraft. Advances in Aerodynamics, Vol. 1, No. 4, pp. 1-21, 2019.
- [13] Li Z.-H., Ma Q., Cui J.-Z. Multi-scale modal analysis for axisymmetric and spherical symmetric structures with periodic configurations. Computer Methods in Applied Mechanics and Engineering, Vol. 317, pp. 1068-1101, 2017.
- [14] Li Z.-H., Ma Q., Cui J.-Z. Second-order two-scale finite element algorithm for dynamic thermosmechanical coupling problem in symmetric structure. Journal of Computational Physics, Vol. 314, pp. 712-748, 2016.
- [15] Christopher O. Johnston. Nonequilibrium Shock-Layer Radiative Heating for Earth and Titan Entry[D]. Virginia Polytechnic Institute and State University, 2006.
- [16] Abhilasha Anna, Iain D. Boyd. Numerical Analysis of Surface Chemistry in High-EnthalpyFlows[J]. Journal of thermophysics and heat transfer, 2015, 29(4): 653-670.
- [17] Antonio Viviani, Giuseppe Pezzella, Salvatore Borrelli. Effect of Finite Rate Chemical Models on the Aerothermodynamics of Reentry Capsules[J]. AIAA-2008-2668, 2008.
- [18] J. Olejniczak, M.J. Wright, J.L. Brown, et al. Computational Modeling of T5 Laminar and Turbulent Heating Data on Blunt Cones, Part 1: Titan Applications[R]. AIAA-2005-0176, 2005.
- [19] Michael J. Wright, Joe Olejniczak, James L. Brown, et al. Computational Modeling of T5 Laminarand Turbulent Heating Data on Blunt Cones, Part 2: Mars Applications[R]. AIAA-2005-177, 2005.
- [20] Barnhardt M., Candler G. V., Detached Eddy Simulation of Hypersonic Base Flows During At-mospheric Entry[R]. AIAA-2006-3575, 2006.
- [21] Lee J. Hun. Basic Governing Equations for the Flight Regimes of Aeroassisted Orbital Transfer Vehicles [R]. AIAA-84-1729, 1984.
- [22] Park C. Problems of Rate Chemistry in the Flight Regimes of Aeroassisted Orbital Transfer Vehicles [J]. Progress In Astronautics and Aeronautics, Vol. 96, pp 511-537, 1985.
- [23] Gupta R. N., Yos J. M., Thompson R. A. A Preview of Reaction Rates and Thermodynamics and Transport Properties for the 11-Species Air Model for Chemical and Thermal Non-Equilibrium Calculations to 30,000K [R]. NASA-TM-101528, 1990.
- [24] Anderson J. D. Hypersonic and High Temperature Gas Dynamics [M]. New York: McGraw-Hill Series in Aeronautical and Aerospace, 1989: 596-599.
- [25] Kang S. W., Jones L. W., Dunn M. G. Theoretical and Measured Electron-Density Distribution at High Altitudes [J]. AIAA Journal, Vol. 11, No. 2, pp 41-149, 1973.
- [26] Blottner F. G. Viscous Shock Layer at the Stagnation Point with Nonequilibrium Air Chemistry [J]. AIAA Journal, Vol. 7, No. 12, pp 2281-2288, 1969.
- [27] Dunn M. G., Kang S. W. Theoretical and Experimental Studies of Reentry Plasmas [R]. NASA-CR-2232, 1973.
- [28] Park C. On Convergence of Computation of Chemically Reacting Flows [R]. AIAA 85-0247, 1985.
- [29] Park C. Nonequilibrium Hypersonic Aerothermodynamics [M]. New York: John Wiley & Sons, 1990: 112-115.

- [30] Park C., Jaffe R. L., Partridge H. Chemical-Kinetic Parameters of Hyperbolic Earth Entry [J]. Journal of Thermophysics and Heat Transfer, Vol. 15, No. 1, pp 76-90, 2001.
- [31] Park C. Two-Temperature Interpretation of Dissociation Rate Data for N2 and O2 [R]. AIAA 88-0458, 1988.
- [32] Park C. Review of Chemical-Kinetic Problems of Future NASA Missions, I: Earth Entries [J]. Journal of Thermophysics and Heat Transfer, Vol. 7, No. 3, pp 385-397, 1993.
- [33] Landrum D., Candler G. Vibration-Dissociation Coupling in Nonequilibrium Flows [R]. AIAA 91-0466, 1991.
- [34] Millikan R. C., White D. R. Systematics of Vibrational Relaxation [J]. Journal of Chemical Physics, Vol. 39, No. 12, pp 3209-3213, 1963.
- [35] Park C. Problems of Rate Chemistry in the Flight Regimes of Aeroassisted Orbital Transfer Vehicles, Thermal Design of Aeroassisted Orbital Transfer Vehicles [J]. Progress in Astronautics and Aeronautics, Vol. 96, pp 511-537, 1985.